

Importance of chiral constraints for the pole content of the $\bar{K}N$ scattering amplitude

P. C. Bruns^a, A. Cieplý^{a,*}

^a*Nuclear Physics Institute of the Czech Academy of Sciences, 250 68 Řež, Czech Republic*

Abstract

We critically examine the $\bar{K}N$ coupled-channel approach presented in [1] and demonstrate that it violates constraints imposed by chiral symmetry of QCD. The origin of this violation can be traced back to the off-shell treatment of the chiral-effective vertices, in combination with the use of non-relativistic approximations and the chosen regularization scheme. We propose an improved version of the approach, which is directly given by a resummation of relativistic Feynman graphs of baryon chiral perturbation theory, and is in accord with the chiral symmetry constraint. Within this improved model, two poles are generated dynamically in the isoscalar $\pi\Sigma - \bar{K}N$ coupled channels sector, in contrast with the non-relativistic model of [1] in which only one such pole was reported.

Keywords: chiral dynamics, meson-nucleon interaction, $\Lambda(1405)$

1. Introduction

The state-of-the-art description of the strangeness $S = -1$ meson-baryon scattering amplitude at low energies is provided by *chirally-motivated* coupled-channel calculations [2, 3, 4, 5, 6, 7, 8] based on solving an integral equation for the scattering amplitude T with a kernel V derived from baryon chiral perturbation theory (BChPT) [9, 10, 11]. The standard low-energy expansion of T is not effective here due to the presence of the $\Lambda(1405)$ resonance just below the antikaon-nucleon threshold [2, 12]. A distinctive result of such approaches is the *two-pole structure* of the dynamically generated $\Lambda(1405)$ [13, 14, 15]. The use of non-perturbative extensions of the standard BChPT framework leads to a notable model-dependence in energy regions where the amplitude is not directly constrained by the existing experimental data, see e.g. [16]. In view of the importance of the antikaon-nucleon scattering amplitude for applications in few- and many-body calculations [17, 18, 19], it is of great interest to assess the model-dependence of the coupled-channel amplitudes in the subthreshold

*Corresponding author

Email address: cieply@ujf.cas.cz (A. Cieplý)

region, and to find further theoretical and experimental constraints to reduce the ambiguities.

In a recent publication [1] (see also [20]), J. Révai criticized a procedure commonly used to simplify the solution of the above-mentioned integral equations, namely, the so-called *on-shell factorisation* which reduces the integral equation to an algebraic equation that can be solved immediately. Solving a Lippmann-Schwinger equation (LSE) without applying this *approximation*, the author of [1] obtained a kernel without energy dependence (an advantageous feature for few-body calculations), and found that the solution “... supports only one pole in the region of the $\Lambda(1405)$ resonance. Thus the almost overall accepted view, that chiral-based interactions lead to a two-pole structure of the $\Lambda(1405)$, becomes questionable” [1]. In the following text we often refer to the work [1] as the JR approach.

In this contribution, we critically examine the model of [1] and the quoted conclusions concerning the $\Lambda(1405)$ structure. We will show that the model strongly violates certain general theoretical constraints derived from chiral symmetry, and thus spoils the motivation to employ a chiral-symmetric kernel from the outset. To make our criticism constructive, we devise a relativistic generalization of the model, henceforth referred to as the BC model, which can also be solved analytically without employing on-shell truncation. Although the resulting model is still not fully satisfactory in some aspects, we show that the pertinent generalized amplitude has an improved chiral behavior, and it brings back a second pole in the isoscalar $\pi\Sigma - \bar{K}N$ threshold region.

The outline of the paper is as follows. In the next section, we briefly review the JR approach presented in [1] and rewrite it in an equivalent and more transparent form that utilizes an effective potential with tadpole integrals accounting exactly for off-shell contributions to the meson-baryon loop function. The approach is improved in Section 3 by adhering to relativistic treatment of the effective potential and constraints arising from chiral symmetry. In Section 4 we provide fits of the model parameters to experimental data and compare the original JR model predictions with those made by the new model. The last section is reserved for concluding remarks.

2. Discussion of the JR approach

Let us focus on the s-wave amplitude for antikaon-nucleon scattering. We shall mostly employ the notation of [1], but leave out the channel indices, anticipating that the building blocks forming the coupled-channel scattering amplitude should thus be considered as matrices in the space of meson-baryon channels whenever appropriate. In particular, the on-shell scattering amplitude T_{on} introduced here is related to the commonly used relativistic s-wave amplitude $f_{0+}(\sqrt{s})$ [21] by

$$f_{0+}(\sqrt{s}) \rightarrow -4\pi^2 \sqrt{\mu} T_{\text{on}}(k) \sqrt{\mu} \quad (1)$$

in the non-relativistic limit. Here \sqrt{s} denotes the total center-of-mass (c.m.) energy of the meson-baryon system, μ is a diagonal channel matrix contain-

ing the reduced masses μ_j of that system, and $k = \sqrt{2\mu(\sqrt{s} - m - M)}$, where m stands for the (diagonal channel-matrix of) meson masses and M for the (diagonal channel-matrix of) baryon masses. We note that momentum k defined this way represents a non-relativistic approximation to the modulus of the c.m. three-momentum \bar{q} given as

$$\bar{q} = \sqrt{(s - (M + m)^2)(s - (M - m)^2)/(2\sqrt{s})}. \quad (2)$$

From coupled-channel unitarity in the space of meson-baryon channels, we should always be able to write our *unitarized* amplitudes (with external particles on-shell) in the generic form

$$\begin{aligned} f_{0+}(\sqrt{s}) &= -[K_{\text{rel}}^{-1} + i\bar{q}]^{-1}, \quad \text{or} \\ 4\pi^2 \sqrt{\mu} T_{\text{on}}(k) \sqrt{\mu} &= [K^{-1} + ik]^{-1}, \end{aligned} \quad (3)$$

where the channel matrices K_{rel}, K are real in the physical region, and specify the chosen model parameterization. In [1], a Lippmann-Schwinger equation (LSE) in the form

$$T(\mathbf{p}', \mathbf{p}; \sqrt{s}) = V(\mathbf{p}', \mathbf{p}; \sqrt{s}) + \int d^3q V(\mathbf{p}', \mathbf{q}; \sqrt{s}) \frac{2\mu}{k^2 - q^2 + i\epsilon} T(\mathbf{q}, \mathbf{p}; \sqrt{s}) \quad (4)$$

is solved for T with a given kernel V . The on-shell s-wave scattering amplitude is then obtained by setting the in- and outgoing meson momenta p, p' on their mass shells, $T_{\text{on}}(k) = T(\mathbf{p}', \mathbf{p}; \sqrt{s})|_{p', p \rightarrow k}$. The debated *on-shell factorisation* corresponds to replacing the loop momentum q in the argument of T and V by its on-shell value k , and subsequently pulling T and V out of the integral to arrive at an algebraic (matrix) equation. This procedure is *not* applied in [1], and so the solution there is somewhat more elaborate.

Following the notation used in [1], we write the loop integrals occurring in the treatment of the LSE as

$$\begin{aligned} G_{AA} &= 8\pi\mu \int_0^\infty dq \frac{q^2(u(q))^2}{k^2 - q^2 + i\epsilon} \\ &= -4\pi^2\mu \left[\frac{\beta}{16} \left(5 - 15(k/\beta)^2 - 5(k/\beta)^4 - (k/\beta)^6 \right) + ik \right] (u(k))^2, \end{aligned} \quad (5)$$

$$G_{AB} = G_{BA} = 8\pi\mu \int_0^\infty dq \frac{q^2(u(q))^2 \gamma(q)}{k^2 - q^2 + i\epsilon} = \bar{\gamma} G_{AA} - I_0, \quad (6)$$

$$G_{BB} = 8\pi\mu \int_0^\infty dq \frac{q^2(u(q))^2 (\gamma(q))^2}{k^2 - q^2 + i\epsilon} = \bar{\gamma}^2 G_{AA} - 2\bar{\gamma} I_0 - I_1, \quad (7)$$

where we introduced

$$I_n := \frac{4\pi}{(2\mu)^n} \int_0^\infty dq q^2 (u(q))^2 (q^2 - k^2)^n, \quad (8)$$

for $n = 0, 1$, and

$$\gamma(q) := \frac{q^2}{2\mu} + m, \quad \bar{\gamma} := \gamma(k), \quad u(q) := \frac{\beta^4}{(\beta^2 + q^2)^2}, \quad (9)$$

with β standing for a cutoff parameter (often referred to as *inverse range*). Then, one can re-write the second equation in (3) as

$$T_{\text{on}}(k) = u(k) \left[\tilde{W}_{\text{JR}}^{-1} - G_{AA} \right]^{-1} u(k), \quad (10)$$

where \tilde{W}_{JR} is again a real coupled-channel matrix depending only on k^2 , and has no branch cuts. Therefore, it cannot contain the unitarity loop function G_{AA} . Indeed, we find that the on-shell s-wave amplitude derived in the JR approach can be brought into the form prescribed by Eq. (10), when the *effective potential* reads

$$\tilde{W}_{\text{JR}} = [\mathbb{1} + \lambda I_0]^{-1} (\bar{\gamma} \lambda + \lambda \bar{\gamma} - \lambda I_1 \lambda) [\mathbb{1} + I_0 \lambda]^{-1}. \quad (11)$$

Here $\mathbb{1}$ denotes the unit matrix in channel space, and the coupling matrix λ was specified in Sec. 2 of [1]. With the amplitude given by Eqs. (10), (11) and the appropriate parameter set, we reproduce exactly the resonance pole positions published in [1]. This way of rewriting the JR solution makes the relation to the *on-shell factorised* approach completely transparent: the latter is obtained by just dropping the terms containing the (diagonal channel matrices of) *tadpole integrals* I_n , a result that can be compared with Eq. (18) in [1]. We also note the explicit results

$$I_0 = \frac{\pi^2 \beta^3}{8}, \quad I_1 = \frac{\pi^2 \beta^3}{16\mu} (\beta^2 - k^2), \quad (12)$$

obtained for the adopted form of $u(q)$, Eq. (9). Other off-shell extrapolations of the elementary vertices, or different regularisation schemes, would lead to different expressions for the functions I_n appearing in the effective potential.

We note that the amplitude constructed above gives scattering lengths which do *not* vanish in the three-flavor chiral limit, as would be required by general arguments following from chiral symmetry and the (pseudo-)Goldstone-boson nature of the lowest meson octet. That is, even though a chiral-symmetric kernel is employed, the non-perturbative resummation framework spoils this attractive feature of the effective theory, inherited from QCD. To illustrate this, let us treat the one-channel case and calculate the corresponding scattering length derived from Eqs. (10), (11). At threshold, where $k = 0$ and $\bar{\gamma} = m$, we obtain

$$a_{0+}^{\text{JR}} = -4\pi^2 \mu \left[\frac{(1 + \lambda I_0)^2}{2\lambda m - \lambda I_1 \lambda} + 4\pi^2 \mu \frac{5\beta}{16} \right]^{-1}. \quad (13)$$

For the on-shell factorised solution with $I_0, I_1 \rightarrow 0$, one gets a prediction in line with the lowest-order ChPT¹. However, if $I_{0,1} \neq 0$, Eq. (13) provides $a_{0+}^{\text{JR}} =$

¹For the multichannel case, we can compare the s-wave scattering lengths following from the threshold limit of the amplitude T_{on} given by Eq. (10) to the known results found in ChPT at the leading order, i.e. neglecting the $\mathcal{O}(m^2)$ contributions, see e.g. [12, 22, 23]:

$$a_{0+,LO}^{\bar{K}N,I=0} = \frac{M_N}{4\pi(M_N + m_K)} \frac{3m_K}{2F_K^2}, \quad a_{0+,LO}^{\bar{K}N,I=1} = \frac{M_N}{4\pi(M_N + m_K)} \frac{m_K}{2F_K^2}.$$

$4\pi^2 m I_1 / (I_0)^2 + \mathcal{O}(m^2)$. Treating I_1 as a quantity of order $\mu^{-1} \sim m^{-1}$, as suggested by Eq. (12), we get an expression of order $\mathcal{O}(m^0)$, forbidden by ChPT. We presume here that the cutoff parameter β stays fixed, or at least it does not vanish in the chiral limit. Therefore, the additional terms $\sim I_n$ which occur when the on-shell truncation is not performed lead to a severe violation of chiral symmetry constraints. From this observation, and similar ones for the multichannel case, we conclude that the effective potential given in Eq. (11) is not *soft* enough in the threshold region to be in accord with fundamental strictures dictated by chiral symmetry. One could argue that the chiral limit is a rather academic notion, not relevant for the physical amplitudes in question. However, as we already stated in the Introduction, theoretical constraints are badly needed in the present situation to reduce the model dependence. If one can construct an improved model, which is more reconcilable with chiral symmetry and does not introduce additional shortcomings, there is no reason to stick to the old model. In the following section, we attempt to devise an improved model with the same cutoff function $u(q)$ as used in [1], but with a *softened* effective interaction kernel of $\mathcal{O}(m)$ at threshold. As we will see, obeying this chiral SU(3) constraint is quite relevant for the pole content of the amplitude.

3. The hybrid BC approach

In an attempt to rectify some shortcomings of the JR approach we modify it by adhering to relativistic hadron kinematics while keeping the loop-integral regularization and not resorting to the *on-shell factorisation*. From the chiral Lagrangian at the leading order, one derives a vertex factor $-ig(\not{q}_i + \not{q}_j)$ for the meson-baryon scattering process $B(p_a)M(q_i) \rightarrow B(p_b)M(q_j)$, where the $p_{a,b}, q_{i,j}$ are off-shell four-momenta, and g is a channel matrix of coupling constants that are related to the λ coefficients introduced in [1]. We multiply the vertex factor with the cutoff functions u defined in Eq. (9) to obtain the new vertex factor

$$u(|\mathbf{q}_j|) \left(-ig(\not{q}_i + \not{q}_j) \right) u(|\mathbf{q}_i|).$$

The modification is not manifestly Lorentz-invariant, so from now on we shall work in the center-of-mass frame, where $p := p_a + q_i = p_b + q_j = (\sqrt{s}, \mathbf{0})$. The summation of s -channel loop graphs (with 0, 1, 2 ... loops) employing this vertex starts as

$$\begin{aligned} -i\mathcal{T}(p_{a,b}, q_{i,j}) &= u(|\mathbf{q}_j|) \left(-ig(\not{q}_i + \not{q}_j) \right) u(|\mathbf{q}_i|) \\ &\quad -iu(|\mathbf{q}_j|)g \int \frac{d^4l}{(2\pi)^4} \frac{(\not{q}_j + \not{l})i(\not{p} - \not{l} + M)(u(|\mathbf{l}|))^2(\not{l} + \not{q}_i)}{((p-l)^2 - M^2)(l^2 - m^2)} gu(|\mathbf{q}_i|) + \dots \end{aligned}$$

It is possible to resum this infinite series in a closed form [24] (see also [25, 26, 27, 28, 29]). Setting the external momenta $p_{a,b}, q_{i,j}$ on shell, the result is

$$\mathcal{T}_{\text{on}}(p_{a,b}, q_{i,j}) = u(\bar{q}) \left[\mathcal{W}^{-1}(\not{p}) - \mathcal{G}(\not{p}, \beta) \right]^{-1} u(\bar{q}), \quad (14)$$

where

$$\mathcal{W}(\not{p}) = [\mathbb{1} + gI_M(\beta)]^{-1} \mathcal{W}_0(\not{p}) [\mathbb{1} + I_M(\beta)g]^{-1}, \quad (15)$$

$$\mathcal{W}_0(\not{p}) = (\not{p} - M)g + g(\not{p} - M) + gI_M(\beta)(\not{p} - M)g, \quad (16)$$

$$\mathcal{G}(\not{p}, \beta) = \int \frac{d^4 l}{(2\pi)^4} \frac{i(u(|\mathbf{l}|))^2 (\not{p} - \not{l} + M)}{((p-l)^2 - M^2)(l^2 - m^2)}, \quad (17)$$

$$I_M(\beta) = \int \frac{d^4 l}{(2\pi)^4} \frac{i(u(|\mathbf{l}|))^2}{(l^2 - m^2)}. \quad (18)$$

Explicit expressions for the loop functions $\mathcal{G}(\not{p}, \beta)$ and $I_M(\beta)$ can be found in Appendix A. It is a standard procedure to compute the partial wave amplitudes of angular momentum $J = \ell \pm \frac{1}{2}$ from an invariant amplitude of the form $\mathcal{T}^{(1)}(s, z)\not{p} + \mathcal{T}^{(0)}(s, z)$, $z = \cos \theta_{\text{cm}}$ [21]. We get

$$\begin{aligned} -16\pi\sqrt{s}f_{\ell\pm}(s) &= \sqrt{E_B + M} \left(\sqrt{s}\mathcal{T}_\ell^{(1)}(s) + \mathcal{T}_\ell^{(0)}(s) \right) \sqrt{E_B + M} \\ &+ \sqrt{E_B - M} \left(\sqrt{s}\mathcal{T}_{\ell\pm 1}^{(1)}(s) - \mathcal{T}_{\ell\pm 1}^{(0)}(s) \right) \sqrt{E_B - M}, \end{aligned} \quad (19)$$

where we used

$$\mathcal{T}_\ell^{(0,1)}(s) = \int_{-1}^1 dz P_\ell(z) \mathcal{T}^{(0,1)}(s, z), \quad E_B = (s + M^2 - m^2)/(2\sqrt{s}).$$

The minus sign on the l.h.s. of Eq. (19) stems from our phase convention for \mathcal{T} . For \mathcal{T} from Eq. (14), the angular integration is trivial, and we arrive at

$$-8\pi\sqrt{s}f_{0+}(s) = \sqrt{E_B + M}u(\bar{q}) \left[\mathcal{W}^{-1}(\sqrt{s}) - \mathcal{G}(\sqrt{s}, \beta) \right]^{-1} u(\bar{q})\sqrt{E_B + M}. \quad (20)$$

Essentially, the Dirac structure matrix \not{p} is just replaced by \sqrt{s} when we go from $\mathcal{T}_{\text{on}}(p_{a,b}, q_{i,j})$ to the partial wave amplitude f_{0+} . The expression for f_{0+} can be cast in a form which is directly comparable to Eqs. (1), (10):

$$f_{0+}^{\text{BC}}(\sqrt{s}) = -4\pi^2\sqrt{\mu} T_{\text{on}}^{\text{BC}}(\sqrt{s})\sqrt{\mu}, \quad (21)$$

$$T_{\text{on}}^{\text{BC}}(\sqrt{s}) = u(\bar{q}) \left[\tilde{W}_{\text{BC}}^{-1}(\sqrt{s}) - G_{AA}^{\text{rel}}(\sqrt{s}) \right]^{-1} u(\bar{q}). \quad (22)$$

Here, within the *relativistic* BC approach, the effective potential and Green function integral read

$$\begin{aligned} \tilde{W}_{\text{BC}}(\sqrt{s}) &= \sqrt{\frac{E_B + M}{\mu}} \frac{\mathcal{W}(\sqrt{s})}{4(2\pi)^3\sqrt{s}} \left[\mathbb{1} + (I_B(\beta) - I_M(\beta)) \frac{\mathcal{W}(\sqrt{s})}{2\sqrt{s}} \right]^{-1} \sqrt{\frac{E_B + M}{\mu}}, \\ G_{AA}^{\text{rel}}(\sqrt{s}) &= 4(2\pi)^3\mu\sqrt{s} I_{MB}(s, \beta). \end{aligned} \quad (23)$$

Again, we refer to Appendix A for the algebraic forms of the relativistic loop integrals I_{MB} , I_M , I_B . Matching of the BC amplitude to the one generated by the JR approach, Eq. (1), at tree level shows that we must have

$$g_{ij} = -\frac{c_{ij}}{4F_i F_j}, \quad (24)$$

where the coupling matrix c_{ij} stems from the λ_{ij} factors introduced in [1]. Eq. (24) represents a correct result as derived from the chiral Lagrangian. Specifically, we have $c_{\bar{K}N, \bar{K}N}^{I=0} = 3$.

The BC amplitude constructed in this section has the advantage that the scattering lengths derived from it are indeed of $\mathcal{O}(m)$. Explicitly, with two open meson-baryon channels, we find for the isoscalar $\bar{K}N$ scattering length

$$a_{0+, \text{BC}}^{\bar{K}N, I=0} = \frac{3m_K b_{0+}^{\bar{K}N, I=0}(m)}{8\pi F_K^2 \left(1 + \frac{m_K}{M_N}\right)}, \quad b_{0+}^{\bar{K}N, I=0}(m) = b_{0+}^{\bar{K}N, I=0}(0) + \mathcal{O}(m), \quad (25)$$

$$b_{0+}^{\bar{K}N, I=0}(0) = \frac{1 - \frac{1}{8} \tilde{I}_M^{(0)}(\beta_{\pi\Sigma}) \left(\frac{29}{2} - 7\tilde{I}_M^{(0)}(\beta_{\pi\Sigma})\right) - \frac{3}{8} \tilde{I}_M^{(0)}(\beta_{\bar{K}N}) \left(1 - \frac{7}{8} \tilde{I}_M^{(0)}(\beta_{\pi\Sigma})\right)^2}{\left[1 - \tilde{I}_M^{(0)}(\beta_{\pi\Sigma}) \left(1 - \frac{21}{32} \tilde{I}_M^{(0)}(\beta_{\bar{K}N})\right) - \frac{3}{4} \tilde{I}_M^{(0)}(\beta_{\bar{K}N})\right]^2},$$

where we introduced the dimensionless quantity $\tilde{I}_M^{(0)}(\beta_j) = I_M^{(m=0)}(\beta_j)/F_0^2$ with the tadpole integrals $I_M(\beta_j)$ and the meson decay constant F_0 both evaluated in the three-flavor chiral limit. The coefficient $b_{0+}^{\bar{K}N, I=0}(m)$ is of $\mathcal{O}(1)$ in the meson-mass expansion, and so the scattering length obviously vanishes in the chiral limit, in line with the strictures imposed by chiral symmetry. It may also be seen from Eq. (25) that the tree-level result of ChPT (see footnote 1) is recovered when the tadpole corrections are dropped. This is in contrast with the JR approach where the I_1 term present in Eqs. (11) and (13) generates a zeroth-order term in the scattering lengths, stemming from the integral G_{BB} in Eq. (7). Indeed, the main problem of the cutoff regularization approach is most directly seen in Eqs. (5)-(7). There, the $\gamma(q)$ factors in the integrands of G_{AB} and G_{BB} , which are formally small, do not lead to a suppression of those integrals with respect to G_{AA} . This is due to polynomial terms containing powers of the cutoff parameter β , which constitutes an additional mass scale that does not vanish in the chiral limit. While the BC approach improves the situation, as its effective potential \tilde{W}_{BC} is *softer* (proportional to $\sqrt{s} - M$) than the one of Eq. (11), an expansion of the threshold amplitudes in m still does not exactly reproduce the $\mathcal{O}(m)$ results of ChPT, since the tadpole integral I_M is non-vanishing in the chiral limit. Had one used dimensional regularization, the mesonic tadpole integrals would be $\sim m^2 \log m$, and the corresponding effective potential would be even softer. It is well known [9] that such power counting problems generally appear when one introduces additional mass scales (like baryon masses or cutoffs) in the low-energy effective theory.

The difference between the JR and BC approaches is demonstrated in Fig. 1, where the pertinent isoscalar $\bar{K}N$ effective potential kernels \tilde{W} are plotted in comparison with the classical Weinberg-Tomozawa (WT) kernel (tadpole integrals I_0 and I_1 set to zero). Apparently, the BC kernel is reasonably close to the WT one while the JR model is significantly off in the whole energy interval relevant for the $\pi\Sigma - \bar{K}N$ physics. In conclusion, the unfortunate combination of the off-shell extrapolation, the chosen regularization scheme and non-relativistic approximations employed in [1] leads to a strong departure from

the leading chiral-symmetric kernel, forcing the *second pole* to move far away from the threshold region. The latter point may become more clear in the next section.

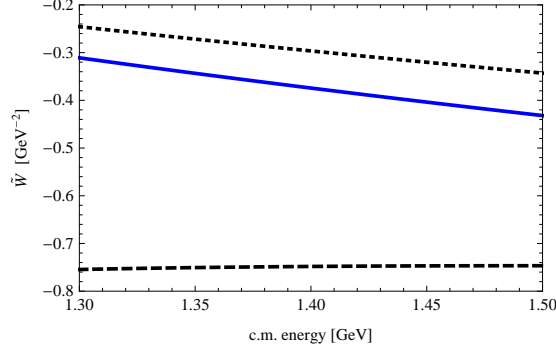


Figure 1: $\bar{K}N(I=0)$ effective kernels over the c.m. energy for the parameters of the model published in [1]. Black dotted - *pure* Weinberg-Tomozawa potential, black dashed - the \tilde{W}_{JR} kernel, blue continuous - the \tilde{W}_{BC} kernel.

4. Results and discussion

The parameters of the chirally motivated approaches are standardly fixed in fits to the available low energy K^-p experimental data that comprise the total cross sections [30, 31, 32, 33, 34, 35], the threshold branching ratios γ , R_c and R_n [36, 37] and the 1s level energy shift and absorption width due to the strong interaction in kaonic hydrogen [38]. In Ref. [1] these observables were calculated treating the isoscalar and isovector sectors separately, adopting different inverse ranges $\beta_{MB}(I=0) \neq \beta_{MB}(I=1)$, though with physical masses used in the $\bar{K}N$ channels to ensure their correct threshold positions. As the latter isospin breaking leads to mixing of the $I=0$ and $I=1$ channels and the parameter space seems too large we adopt a more common approach and perform our calculations with proper physical particle masses and channels (comprising the $\pi\Lambda$, $\pi\Sigma$ and $\bar{K}N$ ones), and assuming $\beta_{MB}(I=0) = \beta_{MB}(I=1)$ as well. In addition, we constrain the fitted meson decay constants by fixing their mutual ratio adopting either $F_K = F_\pi$ or $F_K = 1.193 F_\pi$, the second ratio complying with the PDG [39] as well as lattice results [40] reviews. This leaves us with just 4 fitted parameters (F_π and three β 's) while 7 parameters were used in [1].

The results of our fits are shown in Table 1 in comparison with the original JR model [1] and a version of the CS model [5] restricted to the leading order WT interaction with only two fitted parameters, assuming $F_K = F_\pi$ and a common value $\beta_j = \beta_0$. As a different dataset and fitting approach was used in [5] the χ^2/dof taken from this earlier publication cannot be compared directly with the χ^2/dof obtained for our current models. We also note that no χ^2/dof was provided in [1] but the same author presented χ^2/dof in more extended fits performed later in [20].

Table 1: The fitted meson decay constants and inverse ranges, both in MeV, obtained in fits of low energy K^-p data. Our results for models JR_n and BC_n are shown in comparison with earlier results provided by the CS and JR models. The label n defines a fixed ratio of the meson decay constants, $F_K/F_\pi = 1.193^{n-1}$.

model	F_π	F_K	$I = 0$ sector		$I = 1$ sector			χ^2/dof
			$\beta_{\pi\Sigma}$	$\beta_{\bar{K}N}$	$\beta_{\pi\Lambda}$	$\beta_{\pi\Sigma}$	$\beta_{\bar{K}N}$	
CS [5]	112.8	112.8	701.5	701.5	701.5	701.5	701.5	3.6
JR [1]	73.2	98.3	451.8	830.2	352.4	471.2	934.6	—
JR ₁	116.3	116.3	553.2	860.6	656.3	553.2	860.6	2.62
JR ₂	95.6	114.0	493.6	870.3	536.2	493.6	870.3	2.78
BC ₁	105.9	105.9	876.7	1065.0	773.8	876.7	1065.0	2.39
BC ₂	89.4	106.6	762.2	1125.8	637.8	762.2	1125.8	2.93

The parameter values obtained in our fits are reasonable, in particular the meson decay constants of both BC models and of the JR₂ one are in agreement with predictions of other analyses [40], [41]. In Table 2 we demonstrate how the considered models reproduce the K^-p threshold observables. In general, our models tend to provide a bit too large values for the neutral channels branching ratio R_n and for the kaonic hydrogen absorption width Γ_{1s} . With regards to the latter we find it appropriate to mention that in our fits (and in the χ^2/dof reported in Table 1) we put more weight on the new kaonic hydrogen data and used smaller standard deviations of 20 and 50 eV for the energy shift ΔE_{1s} and the width Γ_{1s} , respectively, instead of the combined statistical and systematical errors reported in [38] and shown in Table 2. In spite of this effort we were not able to bring completely the calculated Γ_{1s} value within the experimental constraints. However, it is a fact that the description of the threshold observables (including the kaonic hydrogen ones) can be improved by accounting for the NLO contact terms in the chiral Lagrangian [4]. These terms were completely disregarded in [1], as well as in the JR_n and BC_n models introduced in the present work. On the other hand, the kaonic hydrogen characteristics predicted by the standard (utilizing *on-shell factorisation*) CS model [5] are within the error bars despite the model is also restricted to the WT interaction kernel and its parameter space is quite narrow, just two parameters adjusted to the data.

The calculated cross sections are shown in Fig. 2 as functions of the initial kaon momenta in the lab system. The upper limit of $p_{LAB} \lesssim 250$ MeV is chosen to guarantee that we can safely neglect any p-wave contributions. Apparently, the models have no problem to reproduce the rather old bubble chamber data taken from Refs. [30, 31, 32, 33, 34, 35]. In fact, the JR₁ and BC₁ model predictions are hard to distinguish in Fig. 2, the only exceptions being the $K^-p \rightarrow \bar{K}^0 n$ and $\pi^- \Sigma^+$ cross sections. We also checked that the JR₂ and BC₂ models provide results completely akin to those provided by the models with $F_K = F_\pi$. In general, both the results presented in Table 2 and Fig. 2 demonstrate that the experimental data are about equally well reproduced by

Table 2: Model predictions for the K^-p threshold branching ratios γ , R_c , R_n [36], [37], and for the strong interaction energy shift ΔE_{1s} and absorption width Γ_{1s} (both in eV) of the 1s level in kaonic hydrogen [38].

	γ	R_c	R_n	ΔE_{1s}	Γ_{1s}
CS	2.36	0.636	0.183	329	643
JR	2.35	0.687	0.203	384	462
JR ₁	2.36	0.647	0.214	261	717
JR ₂	2.36	0.649	0.226	279	709
BC ₁	2.35	0.638	0.215	285	666
BC ₂	2.35	0.642	0.223	294	669
exp	2.36(4)	0.664(11)	0.189(15)	283(42)	541(111)

all considered models.

Further, in Table 3 we present the positions of the isoscalar and isovector poles generated by the models on the second Riemann sheet connected with the physical region by crossing the real axis in between the $\pi\Sigma$ and $\bar{K}N$ thresholds. The JR models provide only one isoscalar pole which appears to be their common feature. In Ref. [1] the one-pole structure is attributed to the fact that one does not resort to on-shell factorisation when dealing with the loop function and the integration is performed over the whole domain of the intermediate meson-baryon off-shell momenta. However, our BC models generate two poles in the $I = 0$ sector demonstrating that the *missing pole* is back when one improves the JR approach by keeping the relativistic form of the effective potential (proportional to $\sqrt{s} - M$). This result confirms the observation already stated in [29]: "The scattering T-matrix without on-shell factorization has two poles in the complex center-of-mass energy plane as with on-shell factorization ...". In fact, the two isoscalar poles also persisted in an earlier work on $\bar{K}N$ interactions [42] that treated the chiral expansion without resorting to on-shell factorisation of the loop function. Of course, the z_2 pole position is very different from where one finds it when the on-shell factorisation is employed, as e.g. in the CS model [5]. While the LO+NLO approach presented in [42] has the z_2 pole shifted to higher energies, the pole is located much farther from the real axis in [29] and the BC models have it close to the $\pi\Sigma$ threshold, either very close to the real axis or even on it (and below the $\pi\Sigma$ threshold). The position of the pole, to which the $\pi\Sigma$ channel couples strongly, is apparently not sufficiently restricted by available experimental data. Thus its varied location within different approaches is not of big concern here. Just for completeness, in Table 3 we also report an isovector z_3 pole found for all considered models at very varied locations, too far to affect physical observables at energies close to the $\bar{K}N$ threshold.

We also checked the sensitivity of the z_2 pole position to the $\beta_{\pi\Sigma}$ value. This parameter is expected to have a significant impact on the appearance and location of the z_2 pole as the $\pi\Sigma$ channel coupling to the pole is large [16]. For the BC₁ model, when the $\beta_{\pi\Sigma}$ parameter is reduced by 10%, the pole shifts to

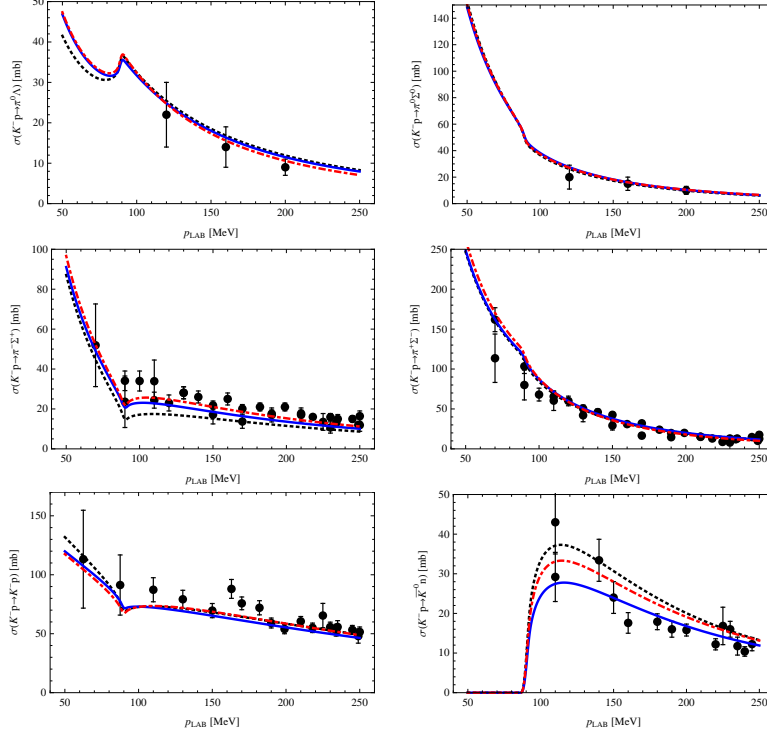


Figure 2: Model predictions for the total cross sections for the $K^-p \rightarrow MB$ reactions. Black dotted - CS model, red dot-dashed - JR₁ model, blue continuous - BC₁ model.

(1326.6, -39.8) MeV, moving rather quickly away from the real axis. When the $\beta_{\pi\Sigma}$ value is increased by 10%, the pole moves to the real axis, to the (1274.9, 0.0) MeV position. Such large variations confirm a strong sensitivity of the z_2 pole position to a particular setting of the BC model and indicate a possible model dependence in general.

To complete our discussion of the model predictions we look at the energy dependence of the elastic K^-p amplitudes generated by the considered models and shown in Fig. 3. There, we have opted for not presenting our models with the $F_K = 1.193 F_\pi$ setting as their inclusion would only make the figure more cluttered. It is remarkable that our JR₁ and BC₁ models provide practically the same K^-p amplitudes for energies $\sqrt{s} \gtrsim 1.4$ GeV. From about 1.42 GeV (1.43 GeV) these models are also in nice agreement with the CS model predictions for the real (imaginary) part of the amplitude. This is in accord with observations made in [16] that the experimental data provide sufficient restrictions to determine the K^-p amplitude around and above the channel threshold irrespective of the adopted theoretical approach. We note that the real part of the K^-p amplitude generated by the original JR model differs even at these energies, most likely due to the different approach to the isospin breaking adopted in [1]. The

Table 3: Pole positions (in MeV) on the $[-,+]$ and $[-,-,+]$ Riemann sheets for the $I = 0$ and $I = 1$ sectors, respectively.

model	z_1 ($I = 0$)	z_2 ($I = 0$)	z_3 ($I = 1$)
CS	(1432.8, -24.9)	(1370.8, -54.2)	(1408.9, -199.7)
JR	(1422.9, -25.7)	—	(1106.5, -71.6)
JR ₁	(1442.8, -23.3)	—	(1141.1, -80.5)
JR ₂	(1441.0, -22.5)	—	(1266.4, 0.0)
BC ₁	(1439.9, -23.3)	(1316.0, -6.76)	(1361.1, -166.9)
BC ₂	(1437.8, -20.9)	(1251.1, 0.0)	(1337.4, -117.3)

differences between various models increase as one goes further below the K^-p threshold into the sector not restricted by experimental data. We do not show the amplitudes below 1.35 GeV in Fig. 3 as the poles emerging close to (and below) the $\pi\Sigma$ threshold have huge impact on the amplitudes generated by some models. In particular, we have noted that the JR, JR₁ and BC₂ models also suffer from emergence of unphysical poles at various Riemann sheets (including the physical one) for energies below the $\pi\Sigma$ threshold. As these energies are too far below the K^-p threshold, the emergence of such spurious states have no impact on physical observables used in our dataset. At the same time, it is difficult to eliminate solutions with very distant poles (i.e. too far from any experimental data points) from the χ^2 fits. Though, it is worth noting that the more established CS model, that utilises the *on-shell factorisation*, behaves quite regularly even at energies below the $\pi\Sigma$ threshold.

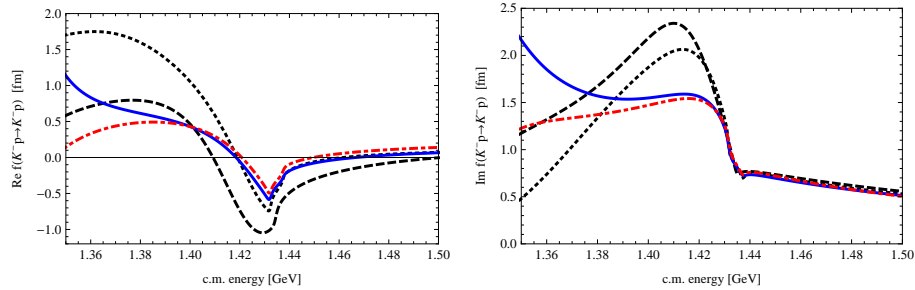


Figure 3: Model predictions for the elastic K^-p amplitude. The real (left panel) and imaginary (right panel) parts of the amplitude generated by our models BC₁ (blue continuous line), and JR₁ (red dot-dashed line) are shown in comparison with the CS model [5] and JR model [1] predictions visualized by the black dotted and dashed lines, respectively.

5. Conclusions

It is always good to scrutinize ad hoc procedures like the *on-shell factorisation*, and to question conclusions based on their use. In this respect, the

study of Ref. [1] is well justified. However, as we point out here, some care has to be taken in the construction of the *chiral-unitarized* model amplitudes, in order not to violate basic constraints from the chiral symmetry of QCD. This symmetry is an important guiding principle of low-energy hadron physics, and yields the motivation to employ kernels derived from chiral-symmetric effective Lagrangians in the model amplitudes. As we have shown, the JR approach of [1] features an effective interaction which deviates strongly from the one derived from the leading chiral Lagrangian, and produces scattering lengths which are not suppressed by powers of the meson masses over the hadronic scale ~ 1 GeV. This happens just due to the inclusion of off-shell effects, which were meant to *improve* the theoretical description. We have provided a way out of this dilemma by explicitly constructing a refined version of the approach, employing relativistic propagators and Feynman rules directly corresponding to the leading chiral Lagrangian, while also avoiding the on-shell truncation. The effective kernel of this new version is much closer to the leading chiral interaction (see Fig. 1), and leaves us with scattering lengths that vanish in the three-flavor chiral limit. Performing simple fits to experimental data with both versions of the model, we have demonstrated that the *chirally improved* version yields two $I = 0$ poles located on the second Riemann sheet in the energy region of the coupled $\pi\Sigma$, $\bar{K}N$ scattering processes, whereas in the non-relativistic model of [1], only one pole is found in the relevant region of the complex-energy surface. While we have used here only the leading term in the chiral expansion of the kernel (Weinberg-Tomozawa interaction) to make a fair comparison with Ref. [1], we believe that the description can be further improved by the inclusion of higher-order interaction kernels, and that the inherent model-dependence can be constrained in a more extended analysis of additional experimental data, e.g. the two-meson photoproduction data from CLAS [43]. Some work in this direction was already done in [44, 45, 7].

Acknowledgement

We thank J. Mareš for careful reading of the manuscript, encouragement and comments. This work was supported by the Czech Science Foundation GACR grant 19-19640S.

Appendix A. Explicit expressions for loop functions

The fundamental loop integrals are defined as follows,

$$I_{MB}(s, \beta) = \int \frac{d^4 l}{(2\pi)^4} \frac{i(u(|\mathbf{l}|))^2}{((p-l)^2 - M^2)(l^2 - m^2)} \Big|_{p=(\sqrt{s}, \mathbf{0})}, \quad (\text{A.1})$$

$$I_M(\beta) = \int \frac{d^4 l}{(2\pi)^4} \frac{i(u(|\mathbf{l}|))^2}{(l^2 - m^2)}, \quad (\text{A.2})$$

$$I_B(\beta) = \int \frac{d^4 l}{(2\pi)^4} \frac{i(u(|\mathbf{l}|))^2}{(l^2 - M^2)}. \quad (\text{A.3})$$

Explicitly, we get

$$I_{MB}(s, \beta) = \frac{(u(\bar{q}))^2}{16\pi^2\sqrt{s}} \left[E_B h_B(\bar{q}, \beta) + E_M h_M(\bar{q}, \beta) - 4\bar{q} \operatorname{Artanh} \left(\frac{2\sqrt{s}\bar{q}}{(M+m)^2 - s} \right) \right], \quad (\text{A.4})$$

where the baryon and meson c.m. energies are

$$E_B = (s + M^2 - m^2)/(2\sqrt{s}), \quad E_M = (s - M^2 + m^2)/(2\sqrt{s}),$$

and the functions appearing in Eq. (A.4) read as

$$h_B(\bar{q}, \beta) = \frac{h_B^{(0)}(\bar{q}, \beta)}{24\beta^4(\beta^2 - M^2)^3} + \frac{h_B^{(1)}(\bar{q}, \beta)}{8\beta^5(\beta^2 - M^2)^{\frac{7}{2}}} \operatorname{Artanh} \left(\frac{\sqrt{\beta^2 - M^2}}{\beta} \right), \quad (\text{A.5})$$

$$\begin{aligned} h_B^{(0)}(\bar{q}, \beta) &= \beta^6(44\beta^4 - 44\beta^2 M^2 + 15M^4) \\ &+ 3\beta^4(24\beta^4 - 10\beta^2 M^2 + M^4)\bar{q}^2 + 3\beta^2(12\beta^4 + 8\beta^2 M^2 - 5M^4)\bar{q}^4 \\ &+ (8\beta^4 + 10\beta^2 M^2 - 3M^4)\bar{q}^6, \end{aligned} \quad (\text{A.6})$$

$$\begin{aligned} h_B^{(1)}(\bar{q}, \beta) &= \beta^6(-16\beta^6 + 24\beta^4 M^2 - 18\beta^2 M^4 + 5M^6) \\ &- 3\beta^4 M^2(16\beta^4 - 16\beta^2 M^2 + 5M^4)\bar{q}^2 - \beta^2 M^2(32\beta^4 - 22\beta^2 M^2 + 5M^4)\bar{q}^4 \\ &- M^2(8\beta^4 - 4\beta^2 M^2 + M^4)\bar{q}^6, \end{aligned} \quad (\text{A.7})$$

$$h_M(\bar{q}, \beta) = \frac{h_M^{(0)}(\bar{q}, \beta)}{24\beta^4(\beta^2 - m^2)^3} + \frac{h_M^{(1)}(\bar{q}, \beta)}{8\beta^5(\beta^2 - m^2)^{\frac{7}{2}}} \operatorname{Artanh} \left(\frac{\sqrt{\beta^2 - m^2}}{\beta} \right), \quad (\text{A.8})$$

$$\begin{aligned} h_M^{(0)}(\bar{q}, \beta) &= \beta^6(44\beta^4 - 44\beta^2 m^2 + 15m^4) \\ &+ 3\beta^4(24\beta^4 - 10\beta^2 m^2 + m^4)\bar{q}^2 + 3\beta^2(12\beta^4 + 8\beta^2 m^2 - 5m^4)\bar{q}^4 \\ &+ (8\beta^4 + 10\beta^2 m^2 - 3m^4)\bar{q}^6, \end{aligned} \quad (\text{A.9})$$

$$\begin{aligned} h_M^{(1)}(\bar{q}, \beta) &= \beta^6(-16\beta^6 + 24\beta^4 m^2 - 18\beta^2 m^4 + 5m^6) \\ &- 3\beta^4 m^2(16\beta^4 - 16\beta^2 m^2 + 5m^4)\bar{q}^2 - \beta^2 m^2(32\beta^4 - 22\beta^2 m^2 + 5m^4)\bar{q}^4 \\ &- m^2(8\beta^4 - 4\beta^2 m^2 + m^4)\bar{q}^6, \end{aligned} \quad (\text{A.10})$$

$$\begin{aligned} I_M(\beta) &= \frac{\beta^4(8\beta^4 + 10\beta^2 m^2 - 3m^4)}{192\pi^2(\beta^2 - m^2)^3} \\ &- \frac{3\beta^3(8\beta^4 m^2 - 4\beta^2 m^4 + m^6)}{192\pi^2(\beta^2 - m^2)^{\frac{7}{2}}} \operatorname{Arcosh} \left(\frac{\beta}{m} \right). \end{aligned} \quad (\text{A.11})$$

Obviously, the explicit expression for the I_B integral can be obtained from I_M by replacing m by M . Finally, in terms of these basic scalar loop functions, the Green function integral $\mathcal{G}(\not{p}, \beta)$ is expressed as

$$\mathcal{G}(\not{p}, \beta) = \frac{\not{p}}{2s} (2\sqrt{s}E_B I_{MB}(s, \beta) + I_M(\beta) - I_B(\beta)) + M I_{MB}(s, \beta). \quad (\text{A.12})$$

We also remind the reader that we are working in the c.m. frame, where $\not{p} = \sqrt{s}\gamma^0$.

References

- [1] J. Révai, *Few Body Syst.* 59 (2018) 49.
- [2] N. Kaiser, P. B. Siegel, W. Weise, *Nucl. Phys.* A594 (1995) 325–345.
- [3] E. Oset, A. Ramos, *Nucl. Phys.* A635 (1998) 99–120.
- [4] Y. Ikeda, T. Hyodo, W. Weise, *Nucl. Phys.* A881 (2012) 98–114.
- [5] A. Cieplý, J. Smejkal, *Nucl. Phys.* A881 (2012) 115–126.
- [6] Z.-H. Guo, J. A. Oller, *Phys. Rev.* C87 (2013) 035202.
- [7] M. Mai, U.-G. Meißner, *Eur. Phys. J.* A51 (2015) 30.
- [8] A. Feijoo, V. Magas, A. Ramos, *Phys. Rev.* C99 (2019) 035211.
- [9] J. Gasser, M. E. Sainio, A. Švarc, *Nucl. Phys.* B307 (1988) 779–853.
- [10] A. Krause, *Helv. Phys. Acta* 63 (1990) 3–70.
- [11] V. Bernard, *Prog. Part. Nucl. Phys.* 60 (2008) 82–160.
- [12] N. Kaiser, *Phys. Rev.* C64 (2001) 045204. [Erratum: *Phys. Rev.* C73, 069902 (2006)].
- [13] J. A. Oller, U.-G. Meißner, *Phys. Lett.* B500 (2001) 263–272.
- [14] D. Jido, J. A. Oller, E. Oset, A. Ramos, U.-G. Meißner, *Nucl. Phys.* A725 (2003) 181–200.
- [15] T. Hyodo, D. Jido, *Prog. Part. Nucl. Phys.* 67 (2012) 55–98.
- [16] A. Cieplý, M. Mai, U.-G. Meißner, J. Smejkal, *Nucl. Phys.* A954 (2016) 17–40.
- [17] N. V. Shevchenko, *Few Body Syst.* 58 (2017) 6.
- [18] S. Ohnishi, W. Horiuchi, T. Hoshino, K. Miyahara, T. Hyodo, *Phys. Rev.* C95 (2017) 065202.
- [19] E. Friedman, A. Gal, *Phys. Rept.* 452 (2007) 89–153.
- [20] J. Révai, *arXiv:1908.08730[nucl-th]* (2019).
- [21] G. F. Chew, M. L. Goldberger, F. E. Low, Y. Nambu, *Phys. Rev.* 106 (1957) 1337–1344.
- [22] Y.-R. Liu, S.-L. Zhu, *Phys. Rev.* D75 (2007) 034003.
- [23] M. Mai, P. C. Bruns, B. Kubis, U.-G. Meißner, *Phys. Rev.* D80 (2009) 094006.

- [24] B. Borasoy, P. C. Bruns, U.-G. Meißner, R. Nisler, Eur. Phys. J. A34 (2007) 161–183.
- [25] J. Nieves, E. Ruiz Arriola, Phys. Rev. D64 (2001) 116008.
- [26] M. F. M. Lutz, E. E. Kolomeitsev, Nucl. Phys. A700 (2002) 193–308.
- [27] D. Djukanovic, J. Gegelia, S. Scherer, Eur. Phys. J. A29 (2006) 337–342.
- [28] P. C. Bruns, M. Mai, U.-G. Meißner, Phys. Lett. B697 (2011) 254–259.
- [29] O. Morimatsu, K. Yamada, Phys. Rev. C100 (2019) 025201.
- [30] M. Csejthey-Barth, et al., Phys. Lett. 16 (1965) 89–91.
- [31] M. Sakitt, T. B. Day, R. G. Glasser, N. Seeman, J. H. Friedman, W. E. Humphrey, R. R. Ross, Phys. Rev. 139 (1965) B719.
- [32] J. K. Kim, Phys. Rev. Lett. 14 (1965) 29.
- [33] T. S. Mast, M. Alston-Garnjost, R. O. Bangerter, A. S. Barbaro-Galtieri, F. T. Solmitz, R. D. Tripp, Phys. Rev. D14 (1976) 13.
- [34] R. O. Bangerter, M. Alston-Garnjost, A. Barbaro-Galtieri, T. S. Mast, F. T. Solmitz, R. D. Tripp, Phys. Rev. D23 (1981) 1484.
- [35] J. Ciborowski, et al., J. Phys. G8 (1982) 13–32.
- [36] R. J. Nowak, et al., Nucl. Phys. B139 (1978) 61–71.
- [37] D. N. Tovee, et al., Nucl. Phys. B33 (1971) 493–504.
- [38] M. Bazzi, et al. (SIDDHARTA), Phys. Lett. B704 (2011) 113–117.
- [39] J. L. Rosner, S. Stone, R. S. Van de Water (Particle Data Group), Phys. Rev. D98 (2018) 030700.
- [40] S. Aoki, et al. (Flavour Lattice Averaging Group), arXiv:1902.08191[hep-lat] (2019).
- [41] M. Tanabashi, et al. (Particle Data Group), Phys. Rev. D98 (2018) 030001.
- [42] M. Mai, U.-G. Meißner, Nucl. Phys. A900 (2013) 51 – 64.
- [43] K. Moriya, et al. (CLAS), Phys. Rev. C87 (2013) 035206.
- [44] L. Roca, E. Oset, Phys. Rev. C87 (2013) 055201.
- [45] S. X. Nakamura, D. Jido, PTEP 2014 (2014) 023D01.